



Degradation and mineralization of aqueous nitrobenzene using ETS-4 photocatalysis

Praveen K. Surolia^{a,b}, Raksh V. Jasra^{a,c,*}

^aDiscipline of Inorganic Materials and Catalysis, Central Salt and Marine Chemicals Research Institute, Council of Scientific and Industrial Research (CSIR), G. B. Marg, Bhavnagar 364002, India, email: suroliapv2004@gmail.com (P.K. Surolia), Tel. +91 265 6693935; Fax: +91 265 6693934; email: rvjasra@gmail.com (R.V. Jasra)

^bSchool of Chemical and Bioprocess Engineering, University College Dublin, Belfield, Dublin 4, Ireland

^cReliance Technology Group, Reliance Industries Limited, Vadodara Manufacturing Division, Vadodara 391346, India

Received 8 September 2014; Accepted 21 July 2015

ABSTRACT

The microporous Engelhard titanosilicate ETS-4 is synthesized with the photocatalytic active –Ti–O–Ti– quantum wires in its framework. The transition metal cations are ion exchanged from their metal salt solutions to give M-ETS-4 (M = Fe, Co, Ni, Cu and Ag). The synthesized materials are extensively characterized by XRD, FT-IR, TGA, SEM and UV–vis-DRS. The photocatalytic activity of these synthesized samples is investigated for the degradation and mineralization of aqueous solution of nitrobenzene as a model pollutant compound. Decrease in chemical oxygen demand (COD) and absorbance of photodegraded NB revealed mineralization of NB. The photocatalytic activity of ETS-4 is attributed to the active –Ti–O–Ti– wires in its framework. Transition metal ions present in ETS-4 enhance the photocatalytic activity by the separating photogenerated charge carriers in ETS-4. Ag ions are found to show pronounced improvement in the photocatalytic activity compared to other transition metal ions. COD study reveals ~59% mineralization in 240 min of irradiation with Ag-ETS-4.

Keywords: Photocatalysis; Mineralization; Degradation; ETS-4; Metal ion exchange; Nitrobenzene; COD

1. Introduction

Undesired by-products with high aromaticity and low biodegradability released from various chemical industries have emerged as major environmental pollutants. These pollutants enter into the environment during their manufacturing processes and their use as chemical intermediates in chemical processes. Decomposition of these by-products to complete mineralization has become one of the major issues in

wastewater pollution. The nitro and amino groups containing aromatics are not only toxic in nature [1–3] but could also inhibit biodegradation of other compounds of wastewater [4–7]. These pollutants cause cyanosis and increased respiratory rate from methaemoglobinemia. Regardless of exposure route or length, they affect the blood as the primary target organ and need to be stringently controlled. Wastewater with nitrobenzene concentrations exceeding 2 mg L⁻¹ is considered hazardous. Various organic chemicals and plastic industries exceed this limit [8]. Due to strong

*Corresponding author.

electron affinity of nitro group, it is resistant to chemical and biological oxidation [9]. The techniques used for nitrobenzene decomposition includes ozonation [10,11], photochemical reduction [12], adsorption [13] and aerobic condition [14].

The photocatalytic reaction has shown advantage over other conventional methods for degradation of organic pollutants from water and air due to its simplicity and complete mineralization based on the generation of highly reactive hydroxyl radicals [15–17]. The photocatalytic decomposition of organic compounds especially from aqueous media has attracted a great deal of attention [7,18–24]. The supporting semiconductor catalysts particularly titania catalyst on silica [25,26], zeolites [27–29], fibre glass [30,31], electrode [32] and cenospheres [33] have also been studied to enhance the photocatalytic activity. However, catalyst recovery due to the leaching of active species remains a challenge even of supported photocatalysts. As a result, research efforts are directed towards developing alternate photocatalytic active materials which are devoid of leaching problem. ETS materials contain chains of $-\text{O}-\text{Ti}^{(\text{IV})}-\text{O}-$ in their framework that exhibit quantum confinement effects and behave as one-dimensional semiconductor nanowires [34–38]. In ETS-4 structure, these chains are found in (0 1 0) direction which are connected by silicate tetrahedral and with titanosilicate “bridging units” in (0 0 1) direction and in the (1 0 0) direction, respectively [39]. ETS-4 has cation-exchange capacity, and transition metal ion- and alkali metal ion-exchanged ETS-4 can be used for catalytic applications. ETS-4 reported in 1989 [40] has effective pore opening around 3–4 Å, that can be adjusted further by systematic contraction through controlled dehydration for various applications such as gas adsorption and separation [35,41–44].

In the present study, the pristine and transition metal ion-exchanged ETS-4 samples are synthesized and their photocatalytic activity for degradation of nitrobenzene under UV-light irradiation is investigated. It has been observed that transition metal ion exchange influences the photocatalytic activity of TiO_2 and supported zeolite materials [45–48]. This has prompted us to investigate the effect of ion exchange on the photocatalytic activity of ETS-4. The transition metal ions are expected to extend the life time of one or both the charge carriers by trapping the charge carrier [49]. For this purpose, the ions to be doped or exchanged must have the work function higher than that of the semiconductor providing a Schottky barrier [29,38,50,51]. Considering this characteristic transition metals, viz., Fe, Co, Ni, Cu and Ag are selected for exchange.

2. Experimental section

2.1. Chemicals and materials

Titanium(IV) butoxide was purchased from Aldrich USA. Sodium silicate was procured from Aquagel, India. Sodium hydroxide (NaOH), Nitrobenzene (NB) and nitrates of all metals were of AR grade purchased from s.d. fine-chem Ltd, India. Deionized water was used to make up the reaction mixture.

2.2. Synthesis of the catalysts

The synthesis of the ETS-4 was carried out as reported earlier [52]. The initial chemical composition of the solution used for ETS-4 synthesis was $\text{Ti}:\text{Si}:\text{Na}:\text{H}_2\text{O}_2:\text{H}_2\text{O} = 0.9:10:14:8:675$ on a molar basis. Titanium (IV) butoxide was added to an aqueous solution of the sodium hydroxide and stirred for 20 min to make the solution homogeneous. The hydrogen peroxide was added to this white colour solution which results in a yellow colour solution. The solution was again stirred for 10 min. The sodium silicate solution (24 wt.% SiO_2 , 8 wt.% Na_2O) was added drop wise to this resultant solution producing a clear bright yellow solution. This solution was stirred for 15 min and transferred to autoclave for hydrothermal synthesis. The hydrothermal synthesis was performed statically at 453 K for 72 h in an autoclave. The powder obtained was filtered, washed with distilled water and dried at 313 K temperature.

For transition metal ion exchange in ETS-4, the weighed amount of ETS-4 (2 g) was stirred for 24 h with the metal salt solution in 100 ml water having concentration calculated for 0.5% (w/w) metal ion exchange at room temperature. In the ion exchange, Na ions would be replaced by transition metal ions from ETS-4. After the ion exchange, the samples were washed with distilled water, filtered and dried at 393 K for 12 h. The samples were calcined at 723 K. The obtained samples were named as M-ETS-4, where M represents the exchanged transition metal.

2.3. UV irradiation experiments

The catalytic reaction was carried out in a reactor consisting of two parts as reported earlier [53]. The first part consisting of an inner quartz double-wall jacket with water circulation facility and second part an outer borosilicate glass container (volume 250 ml after insertion of the inner part) in which the reaction takes place. The 125-W mercury vapour lamp (Crompton Greaves Ltd, India) was used for the UV irradiation source and placed in an empty chamber at the centre of inner

quartz double-wall jacket. The reaction mixture was continuously stirred by keeping a magnetic stirrer below the reactor. Photocatalytic activity was studied at pH of 6.9 of the initial reaction mixture and pH was not adjusted during the experiments. The temperature of reaction was maintained at 293 K for all the reactions. The photocatalytic activity of the catalysts was evaluated by measuring the decrease in concentration of nitrobenzene in the reaction aqueous solution using UV–visible spectroscopy. The calibration curve was plotted for nitrobenzene using standard samples of known concentration (5, 10, 20, 30, 40 and 50 ppm) of nitrobenzene in distilled water. The slope of the curve was calculated and used for determining nitrobenzene concentration using Beer–Lambert's law.

Prior to commencing irradiation, a suspension containing 50 mg of the catalyst and 250 ml of aqueous solution of ca. 50 ppm of nitrobenzene was stirred continuously for 30 min in the dark. The sample was analysed to measure the adsorption of nitrobenzene on the catalyst surface. Five millilitre reaction samples were withdrawn for analysis by a syringe from the irradiated suspension at intervals of 10 min for the first hour and every hour thereafter. The catalysts were separated by centrifugation from the aqueous solution and concentration was determined by UV–visible spectrophotometer (Cary 500, Varian, Palo Alto, CA). The absorbance was measured at λ_{\max} 267 nm for nitrobenzene. The mineralization of nitrobenzene in aqueous solution was confirmed by chemical oxygen demand (COD) analysis of the samples taken at different reaction time intervals. COD is an index of water pollution by organics and COD differences with irradiation time are exclusively related to the degree of oxidation of the organic matter [22,54–56].

2.4. Catalyst characterization

X-ray diffraction data were measured at ambient temperature using a Phillips X'pert MPD system employing $\text{CuK}\alpha 1$ ($\lambda = 0.15405$ nm) radiation at 295 K. Diffraction patterns were taken over the range of 5° – 60° 2θ at the scan speed of $0.1^\circ \text{sec}^{-1}$. The crystallinity of the catalysts was calculated with reference to pristine ETS-4 by taking the average of 8 major peaks of the catalyst ($2\theta = 7.5, 12.7, 16.7, 19.9, 24.7, 30.0, 50.7$ and 52.1). The band gap energy of the catalysts was determined using the diffuse reflectance spectroscopy (DRS). The spectrophotometer (Shimadzu UV-3101PC) was equipped with an integrating sphere and BaSO_4 was used as a reference. The spectra were recorded at room temperature in the wavelength range of 225–700 nm. The band gap energy of catalysts was calculated according to the equation:

$$\text{Band gap (EG)} = hc/\lambda \quad (1)$$

where EG is the band gap energy (eV), h the Planck's constant, c the light velocity (m/s) and λ is the wavelength (nm).

The FT-IR spectroscopic measurements were carried out using Perkin-Elmer GX spectrophotometer. The spectra were recorded in the range 500 – $4,000$ cm^{-1} with a resolution of 4 cm^{-1} as KBr pellets. The morphology of the synthesized catalysts particles and presence of metal was studied using Scanning Electron Microscope (Leo Series VP1430) equipped with INCA, Energy Dispersive System (EDX), Oxford instruments. The sample powder was supported on aluminium stubs prior to measurement. Thermogravimetry and differential thermal analysis were performed on a TGA/SDTA851^e, METTLER TOLEDO system in a temperature range of 30 – 750°C with a heating rate of 5°C min^{-1} under an air stream.

3. Results and discussion

3.1. Structural, textural and electronic properties

The powder XRD patterns of pristine and of the ion-exchanged ETS-4 catalysts are shown in Fig. 1(a) and compared with literature reports. The patterns of ion-exchanged catalysts are similar to that of pristine ETS-4 and are in good agreement for the peaks at their respective 2θ values. This suggests that the structure of ETS-4 is retained after metal ion exchange and no impurity of silica or transition metal oxides occurred during metal ion exchange. The crystallinity was found to decrease with transition metal ion exchange (Table 1). The major diffraction lines for as-synthesized ETS-4 were indexed with an orthorhombic unit cell with space group symmetry of Cmmm and cell parameters $a = 23.2422$ Å, $b = 7.2021$ Å, $c = 6.9324$ Å and $\alpha = \beta = \gamma = 90^\circ$ shown as in Table 1. The reported cell parameters in previous studies are $a = 23.2272$ Å, $b = 7.1751$ Å, $c = 6.9727$ Å and $a = 23.24$ Å, $b = 7.23$ Å, $c = 6.95$ Å, respectively [35,57]. The calculated lattice constants of ETS-4 were found to decrease with increase in the metal ion content which supports the exchange of transition metal ions in the lattice.

The IR absorbance spectra of the samples were recorded in the frequency range 500 – $4,000$ cm^{-1} (Fig. 1(b)). The absorbance values at around $3,590$, $3,443$ and $3,216$ cm^{-1} are due to stretching vibrations, while at $1,650$ cm^{-1} is due to the bending vibration of water molecules and OH groups present at the surface [35,58]. The absorbance at $1,136$ cm^{-1} is due to asymmetric stretching vibrations of Si–O–Si bridges, while peaks at

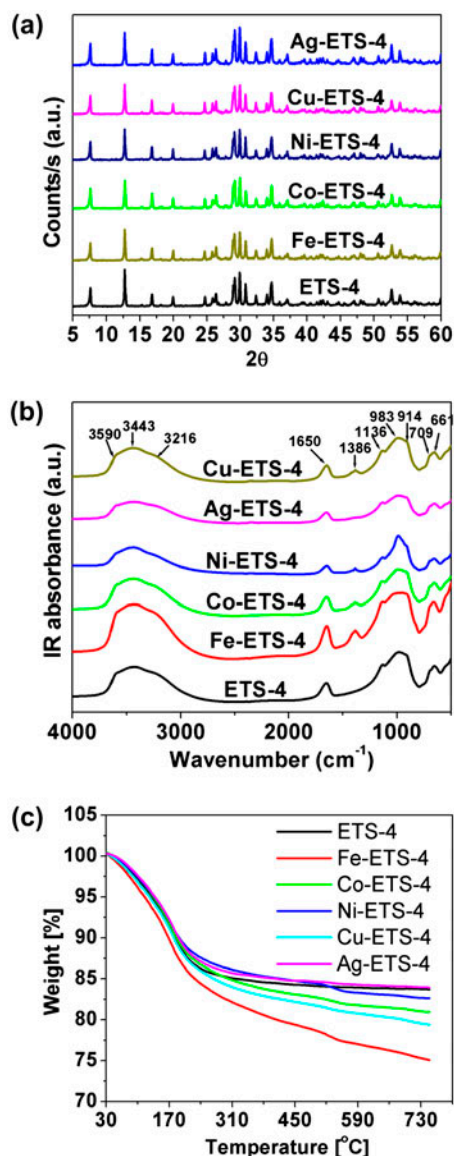


Fig. 1. XRD patterns (a), FT-IR spectra (b) and TGA patterns (c) of pristine and metal ion-exchanged ETS-4 catalysts.

983 and 914 cm^{-1} are the resultant of Si–O–Ti stretching vibrations. The stretching and bending vibrations of Ti–O–Ti give rise to the absorption peak at 704 and 661 cm^{-1} , respectively. The comparison of the IR spectra of pristine and transition metal-exchanged ETS-4 show that there is an additional peak at around 1,386 cm^{-1} in the IR spectra of transition metal-exchanged ETS-4. This peak results from vibrations of H^+ ion [59]. This Brønsted acidity arises due to the cluster formation of the hydroxyl group with transition metal ion and leaving behind free H^+ ion in the framework.

The water loss curves determined by thermal gravimetric analysis for as-synthesized and transition

metal-exchanged ETS-4 are given in Fig. 1(c) which show the maximum weight loss between 100 and 200°C. The weight loss is attributed to removal of physisorbed water molecules [60,61]. The figure shows that Ni and Ag metal exchange exhibit weight loss approximately 17 and 16%, respectively, which are similar to pristine ETS-4 (~18% weight loss). Fe, Co and Cu ion-exchanged samples show the decrease in the stability as seen in higher weight loss 25, 20 and 21%, respectively. The higher weight loss suggests a more hydrated framework in the material. The higher weight loss with these metal-exchanged ETS-4 is because of the removal of strongly bounded water which causes the structure to collapse [60]. This can also be seen from the loss of crystallinity of these catalysts.

The band gap from diffuse reflectance measurement for pristine ETS-4 was calculated 3.8 eV (Table 1). The transition metal-exchanged ETS-4 catalysts showed two band gaps. The values of these band gaps were same for all the samples. It seems that the band gap of ETS-4 is apparently blue-shifted compared to that of TiO_2 bulk (~3.2 eV). This blue shift in ETS-4 catalyst from TiO_2 bulk is attributable to the quantum size effect of the –Ti–O–Ti–O– nanowires embedded in the ETS-4 crystalline matrix [61] which arises from the confinement of charge carriers in a nanosized semiconductor [39]. The second absorption edge and new broad visible absorption bands [62] for the exchanged and bimetallic materials in metal ion-exchanged ETS-4 is attributed to the excitation of 3d electrons to the conduction band of –Ti–O–Ti–O– semiconductor nanowires (charge-transfer transition) [63–65].

The SEM image presented in Fig. 2 shows the crystals of the pristine and transition metal exchanged ETS-4 in the form of intergrown and intertwined aggregates of plates as reported earlier [59,66]. All the catalysts are having identical morphology and the SEM images revealed that the pristine ETS-4 and M-ETS-4 are indistinguishable suggesting insignificant effect of transition metal exchange on the morphology of synthesized catalysts. The amount of exchanged transition metal ion was estimated by EDAX analysis of the synthesized catalysts. The amount of the Na, Ti and exchanged metal is given in Table 1. The ratio of Na to Ti was found to decrease after the transition metal ion exchange confirming metal ion exchange with the Na ion. The EDAX analysis confirms the presence of transition metal ions in these samples as per calculation.

3.2. Photocatalytic activity

The photocatalytic activities of the synthesized catalysts were monitored at constant catalyst dose of 200 mg L^{-1} and 293 K temperature, while initial

Table 1
Structural and electronic properties of the catalysts

Catalyst	Crystallinity (%)	Lattice constants (Å)			Na/Ti	% Metal (EDX)	Band gap (eV)
		<i>a</i>	<i>b</i>	<i>c</i>			
ETS-4	100	23.2422	7.2021	6.9324	1.97	–	3.8
Fe-ETS-4	85	23.2420	7.1963	6.9187	1.67	0.74	4.0/3.6
Co-ETS-4	95	23.1635	7.1926	6.9182	1.93	0.50	4.0/3.6
Ni-ETS-4	89	23.2345	7.2000	6.9246	1.72	0.52	3.9/3.5
Cu-ETS-4	84	23.1543	7.1950	6.9252	1.62	0.63	4.0/3.5
Ag-ETS-4	96	23.1945	7.1950	6.9264	1.60	0.47	3.9/3.5

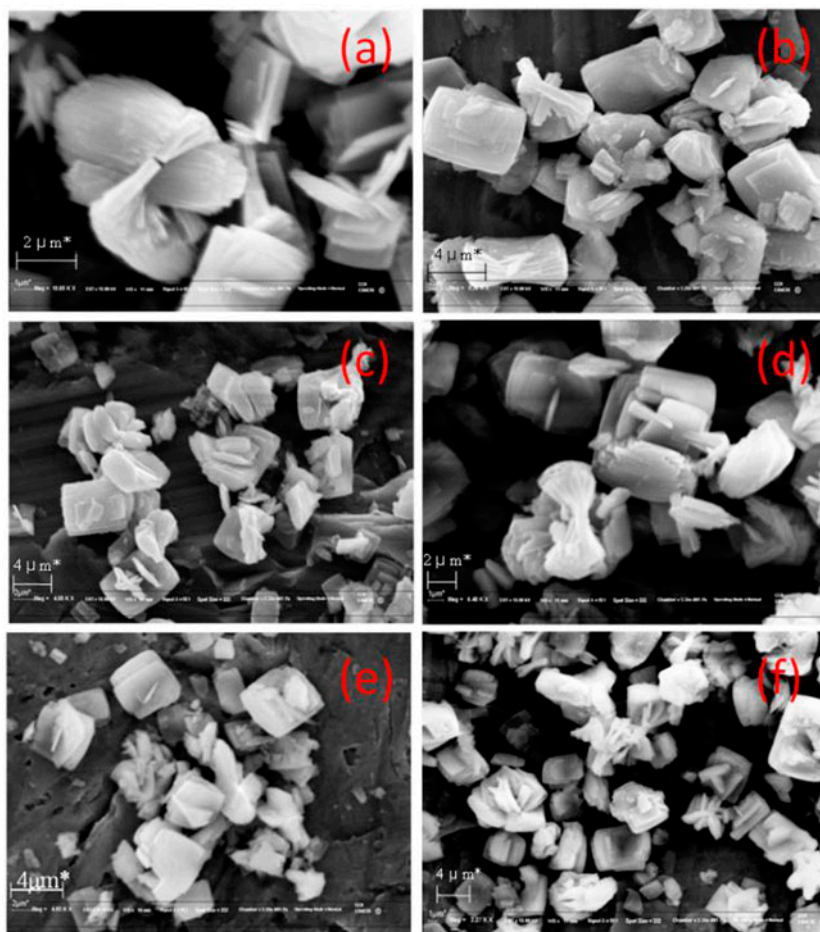


Fig. 2. SEM images of pristine ETS-4 (a), Fe-ETS-4 (b), Co-ETS-4 (c), Ni-ETS-4 (d), Cu-ETS-4 (e) and Ag-ETS-4 (f) catalysts.

concentration of nitrobenzene was 50 ppm. Fig. 3(a) shows the molar concentration vs. time graph

The initial rates of photocatalytic degradation calculated for all catalysed reactions are given in Table 2. Initial rates reveal that M-ETS-4 are more active catalysts than pristine ETS-4 and Ag-ETS-4

showed highest catalytic activity among all metal ion-exchanged ETS-4 catalysts. Fig. 3(b) shows the changes in absorption spectra of nitrobenzene with Ag-ETS-4 under UV-light irradiation. Nitrobenzene shows maximum absorbance at 267 nm and the decrease in concentration calculated by the absorbance at this

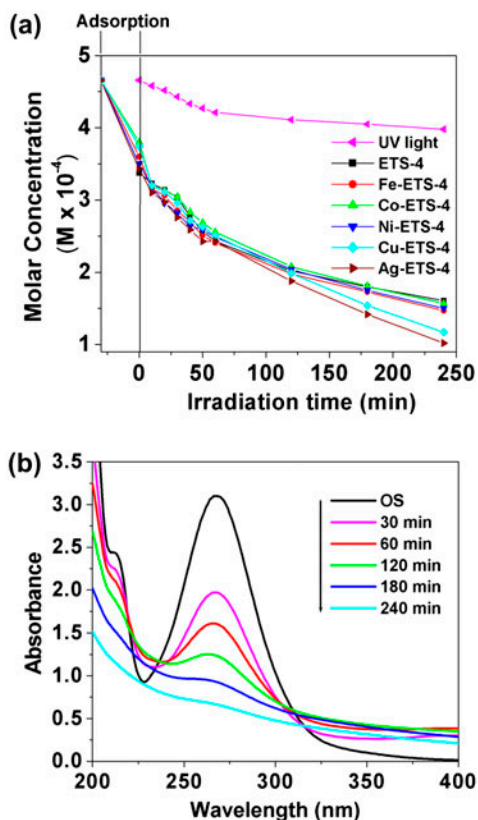


Fig. 3. Photocatalytic disappearance of nitrobenzene using different catalysts (a) and UV-visible absorbance spectra of different reaction samples taken with Ag-ETS-4 catalyst (b).

wavelength Fig. 3(b) shows the degradation of nitrobenzene, and was used as a measure of photocatalytic activity.

Factors which govern the degradation are (i) generation and migration of the photogenerated e^-/h^+ pair, and (ii) reaction between these photogenerated h^+ (OH^\cdot radical) and organic substrate molecules. These both processes occur in series and each step may become the rate-determining step for overall process. Initially, at high concentration of NB former process dominates, resulting lower difference in degradation

values. After first hour of reaction where NB concentration becomes low due to degradation, the latter process dominates, resulting high degradation values. Due to these factors, catalysts performance can easily be distinguished at lower substrate concentration as seen in Fig. 3(a). Initial high concentration reduces the diffusion rate of intermediates from the catalyst surface as well as the transfer rate of the substrate towards catalyst which is another reason for similar performance of all the catalysts in first hour of reaction [67].

The percentage degradation of nitrobenzene after 4 h reaction is shown in Fig. 4(a). The transition metal ion exchanged ETS-4 samples exhibit higher activity than pristine ETS-4. The percentage degradation observed after 4 h reaction time was 65, 69, 67, 68, 75 and 79 for pristine, Fe, Co, Ni, Cu and Ag metal ion-exchanged ETS-4, respectively. Moreover, Ag-ETS-4 catalyst showed highest photocatalytic degradation (79%) among all other transition metal-exchanged ETS-4 catalysts. However, Ag ion-exchanged TiO_2 was used as a photocatalyst under the similar reaction conditions had shown 89% degradation of NB in earlier study [29]. The amount of TiO_2 in the ETS-4 catalyst calculated as per its stoichiometry is 17%. Thus, the amount of photocatalytic active species ($-O-Ti^{(IV)}-O-$) of the prepared catalyst in 50 mg is 8.5 mg. The earlier observed higher activity of TiO_2 can be explained by the higher number of available surface $TiOH$ groups and by the fact that most of the photons are able to activate the band gap mechanism for TiO_2 [68]. Considering this, the results obtained with ETS-4 material as a photocatalyst are very promising. For comparison, an experiment was carried out with commercially available TiO_2 (Degussa P25) without further modification and only 61% degradation of nitrobenzene was observed. This confirms the superior performance of ETS-4 catalysts. The percentage decrease in the concentration due to adsorption in dark was found to be 28, 23, 19, 25, 20 and 26 for pristine ETS-4, Fe, Co, Ni, Cu and Ag metal-exchanged ETS-4 catalyst, respectively. The decrease in the nitrobenzene concentration only due to UV irradiation in absence of catalyst was found nearly 14%. The COD analysis of the reaction mixture

Table 2

Kinetics of the aqueous nitrobenzene photocatalytic degradation using ETS-4 based catalysts

Catalyst	Initial rate $\times 10^6$ (mol l^{-1} sec $^{-1}$)	Standard redox potential E^0 (V) of metal
ETS-4	4.6	-2.71 (Na)
Fe-ETS-4	5.1	+0.33
Co-ETS-4	5.3	-0.28
Ni-ETS-4	5.8	-0.25
Cu-ETS-4	4.8	+0.68
Ag-ETS-4	6.1	+0.80

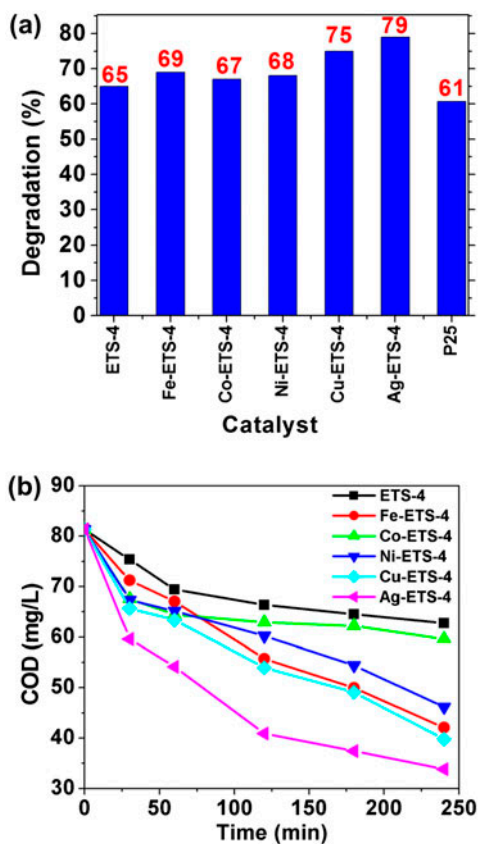


Fig. 4. Photocatalytic disappearance of nitrobenzene after 4 h irradiation (a) and Reduction in COD value (b) using different synthesized catalysts.

samples at different time intervals determined the complete mineralization of nitrobenzene during the degradation process, Fig. 4(b). Approximately 59% mineralization was observed in 240 min with Ag-ETS-4 catalyst which is best among all samples used. The reaction sample was analysed by inductively coupled plasma (ICP) analysis after the reaction. The absence of exchanged metals in the reaction sample confirms the lack of leaching of these metals during the reaction.

The silver metal-exchanged ETS-4 showed the highest activity for both degradation and mineralization. Furthermore, all the metal-exchanged ETS-4 catalysts showed enhanced photocatalytic activity. The transition metal can capture the photogenerated electrons in the $-\text{O}-\text{Ti}^{(\text{IV})}-\text{O}-$ semiconductor nanowires under UV-irradiation to be reduced to M^0 . The effect of transition metal ion exchange on TiO_2 -based photocatalysts has been extremely studied and the capture of photogenerated electrons by transition metals over TiO_2 -based photocatalysts is well known to occur. Similar effect may also be possible for $-\text{O}-\text{Ti}^{(\text{IV})}-\text{O}-$

nanowires present in the ETS-4 system. The contact of a metal with a semiconductor creates a heterojunction at the interface with the difference in electrochemical potential of both the surfaces, set by their position of work function (ϕ_m) and Fermi level (E_F), respectively. The contact between these two phases leads to the electron flow from the phase with more negative initial electrochemical potential to the other until the electrochemical potentials of both phases are in equilibrium, in this case from the semiconductor to the contacting phase. A barrier height (ϕ_b), known as Schottky barrier, is formed at the interface which stops the back transfer of electron and the barrier height energy ($q\phi_b$) is the differences between the equilibrium Fermi level and the energy of the conduction band edge (Fig. 5):

$$\phi_b = (\phi_m - \chi_s)/q \quad (2)$$

where ϕ_m is the work function of the metal (in eV) and χ_s is the electron affinity of the semiconductor.

The conduction band energy level of TiO_2 (E_c) is approximately -0.3 eV [69] and thus $-\text{O}-\text{Ti}^{(\text{IV})}-\text{O}-$ semiconductor unit of ETS-4 is higher than that of reduction potential of transition metal as shown in Table 2. This difference in the energy level makes it feasible to thermodynamically transfer an e^- from conduction band to metallic particles and the Schottky barrier at the interface that makes the trapping this electron feasible. Thus, by the trapping of electron, these transition metal acts as a sink for photogenerated electrons and minimize the e^-/h^+ recombination to assist the photocatalytic oxidation of nitrobenzene with known oxidizing species such as free h^+ or OH^\cdot radicals [70]. OH^\cdot radical is an extremely important species responsible for the photocatalytic oxidation of organic compounds [71–73]. On the other hand, Na^+ and K^+ ions in the pristine ETS-4 cannot be reduced into Na and K metal by photogenerated e^- as the reduction potentials of these ions are much higher (Table 2); this causes the lower photocatalytic activity of ETS-4 towards nitrobenzene degradation.

ETS-4 consists of a combination of four polymorphs, which causes the appearance of numerous stacking faults blocking the 12-membered rings channels, and thus the effective pore size of as-synthesized ETS-4 is ca. 3.7 Å, which may be even smaller for transition metal ion-exchanged ETS-4. Hence, the reaction of nitrobenzene most likely takes place on the external surface of pristine and M-ETS-4 materials, where defect sites may be abundant [68]. The photocatalytic active sites are titanol species located on the external surfaces where the $-\text{O}-\text{Ti}-\text{O}-\text{Ti}-$ chain emerges, exposing a surface $\text{Ti}-\text{OH}$ titanol group [68].

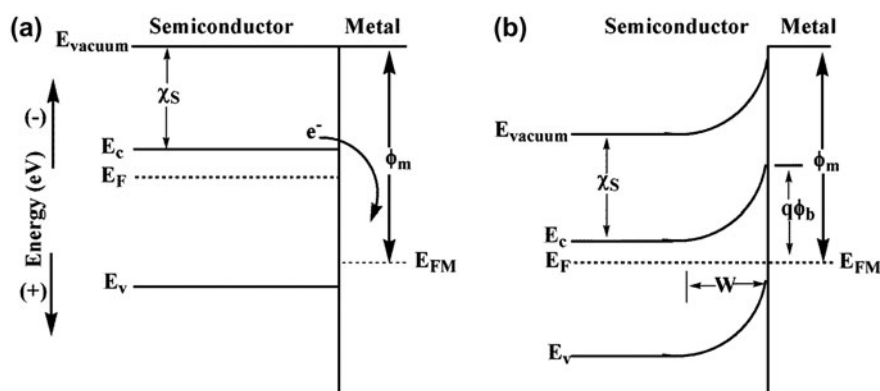


Fig. 5. Band bending diagram for n-type semiconductor/metal junction (a) before equilibrium and (b) at equilibrium.

4. Conclusions

The microporous ETS-4 is found to exhibit photocatalytic activity under UV light and exhibits a promise as an alternative to conventional supported titania photocatalysts. Decrease in COD and absorbance of photodegraded NB revealed mineralization of NB. The transition metal ion-exchanged ETS-4 zeolites show enhanced activity for the photocatalytic degradation as well as mineralization of nitrobenzene from aqueous solution compared to pristine ETS-4. The photocatalytic activity shown by ETS-4 was due to the presence of $\text{-O-Ti}^{(IV)\text{-O-}}$ nanowires in its structure. The enhanced activity of the transition metal-ion exchanged ETS-4 is found to be due to transition metal acting as a sink for photogenerated electrons. Ag ions show pronounced effect to improve the photocatalytic activity compared to other transition metals. The Ag-ETS-4 catalyst exhibited maximum photodegradation, mineralization (~59% COD decrease) and higher initial rates than pristine ETS-4 and among all other transition metal-exchanged ETS-4 catalysts. Considering the amount of photocatalytic active part (17%) in the synthesized ETS-4 material, the observed results are satisfactory and further research for the modification in this existing material is needed to enhance its photocatalytic activity. Microporous zeolite ETS-4 having chains of $\text{-O-Ti}^{(IV)\text{-O-}}$ semiconductor units as photocatalyst can provide an alternate of conventional supported photocatalyst to solve the leaching problem.

Acknowledgements

This work was supported by Council of Scientific and Industrial Research, New Delhi, India under the Junior Research Fellowship Scheme (F. No. 10-2(5)/2005(i)-E.U.II).

References

- [1] S. Ikeda, N. Sugiyama, B. Pal, G. Marci, L. Palmisano, H. Noguchi, K. Uosaki, B. Ohtani, Photocatalytic activity of transition-metal-loaded titanium(IV) oxide powders suspended in aqueous solutions: Correlation with electron-hole recombination kinetics, *Phys. Chem. Chem. Phys.* 3 (2001) 267–273.
- [2] A. Fuerte, M.D. Hernández-Alonso, A.J. Maira, A. Martínez-Arias, M. Fernández-García, J.C. Conesa, J. Soria, Visible light-activated nanosized doped-TiO₂ photocatalysts, *Chem. Commun.* (2001) 2718–2719.
- [3] B.E. Haigler, J.C. Spain, Biotransformation of nitrobenzene by bacteria containing toluene degradative pathways, *Appl. Environ. Microbiol.* 57 (1991) 3156–3162.
- [4] L.E. Hallas, M. Alexander, Microbial transformation of nitroaromatic compounds in sewage effluent, *Appl. Environ. Microbiol.* 45 (1983) 1234–1241.
- [5] E.M. Davis, H.E. Murray, J.G. Liehr, E.L. Powers, Basic microbial degradation rates and chemical byproducts of selected organic compounds, *Water Res.* 15 (1981) 1125–1127.
- [6] M. Rodriguez, V. Timokhin, F. Michl, S. Contreras, J. Gimenez, S. Esplugas, The influence of different irradiation sources on the treatment of nitrobenzene, *Catal. Today* 76 (2002) 291–300.
- [7] P.K. Surolia, M.A. Lazar, R.J. Tayade, R.V. Jasra, Photocatalytic degradation of 3,3'-dimethylbiphenyl-4,4'-diamine (o-tolidine) over nanocrystalline TiO₂ synthesized by sol-gel, solution combustion, and hydrothermal methods, *Ind. Eng. Chem. Res.* 47 (2008) 5847–5855.
- [8] Y. Mu, R.A. Rozendal, K. Rabaey, J. Keller, Nitrobenzene removal in bioelectrochemical systems, *Environ. Sci. Technol.* 43 (2009) 8690–8695.
- [9] J.D. Rodgers, N.J. Bunce, Treatment methods for the remediation of nitroaromatic explosives, *Water Res.* 35 (2001) 2101–2111.
- [10] A. Latifoglu, M.D. Gurol, The effect of humic acids on nitrobenzene oxidation by ozonation and O₃/UV processes, *Water Res.* 37 (2003) 1879–1889.
- [11] F.J. Beltrán, J.M. Encinar, M.A. Alonso, Nitroaromatic hydrocarbon ozonation in water. 1. Single ozonation, *Ind. Eng. Chem. Res.* 37 (1998) 25–31.

- [12] O.V. Makarova, T. Rajh, M.C. Thurnauer, A. Martin, P.A. Kemme, D. Cropek, Surface modification of TiO₂ nanoparticles for photochemical reduction of nitrobenzene, *Environ. Sci. Technol.* 34 (2000) 4797–4803.
- [13] S.A. Boyd, G. Sheng, B.J. Teppen, C.T. Johnston, Mechanisms for the adsorption of substituted nitrobenzenes by smectite clays, *Environ. Sci. Technol.* 35 (2001) 4227–4234.
- [14] C. Zheng, J. Zhou, J. Wang, B. Qu, J. Wang, H. Lu, H. Zhao, Aerobic degradation of nitrobenzene by immobilization of *Rhodotorula mucilaginosa* in polyurethane foam, *J. Hazard. Mater.* 168 (2009) 298–303.
- [15] D.F. Ollis, E. Pelizzetti, N. Serpone, Photocatalyzed destruction of water contaminants, *Environ. Sci. Technol.* 25 (1991) 1522–1529.
- [16] M.R. Hoffmann, S.T. Martin, W.Y. Choi, D.W. Bahnemann, Environmental applications of semiconductor photocatalysis, *Chem. Rev.* 95 (1995) 69–96.
- [17] J. Peral, X. Doménech, D.F. Ollis, Heterogeneous photocatalysis for purification, decontamination and deodorization of air, *J. Chem. Technol. Biotechnol.* 70 (1997) 117–140.
- [18] M.A. Fox, K.E. Doan, M.T. Dulay, The effect of the “Inert” support on relative photocatalytic activity in the oxidative decomposition of alcohols on irradiated titanium dioxide composites, *Res. Chem. Intermed.* 20 (1994) 711–721.
- [19] Y. Kim, M. Yoon, TiO₂/Y-Zeolite encapsulating intramolecular charge transfer molecules: A new photocatalyst for photoreduction of methyl orange in aqueous medium, *J. Mol. Catal. A: Chem.* 168 (2001) 257–263.
- [20] S.K. Lee, A. Mills, Detoxification of water by semiconductor photocatalysis, *J. Ind. Eng. Chem.* 10 (2004) 173–187.
- [21] A. Mills, S.K. Lee, A web-based overview of semiconductor photochemistry-based current commercial applications, *J. Photochem. Photobiol., A Chem.* 152 (2002) 233–247.
- [22] D. Chakraborty, S. Sen Gupta, Decolourisation of Metanil Yellow by visible-light photocatalysis with N-doped TiO₂ nanoparticles: Influence of system parameters and kinetic study, *Desalin. Water Treat.* 52 (2013) 5528–5540.
- [23] C.D. Wu, J.Y. Zhang, Y. Wu, G.Z. Wu, Degradation of phenol in water by the combination of sonolysis and photocatalysis, *Desalin. Water Treat.* 52 (2014) 1911–1918.
- [24] B. Sarwan, B. Pare, A.D. Acharya, S.B. Jonnalagadda, Mineralization and toxicity reduction of textile dye neutral red in aqueous phase using BiOCl photocatalysis, *J. Photochem. Photobiol., B Biol.* 116 (2012) 48–55.
- [25] M. Anpo, H. Nakaya, S. Kodama, Y. Kubokawa, K. Domen, T. Onishi, Photocatalysis over binary metal oxides. Enhancement of the photocatalytic activity of titanium dioxide in titanium-silicon oxides, *J. Phys. Chem.* 90 (1986) 1633–1636.
- [26] S. Sato, Effects of surface modification with silicon oxides on the photochemical properties of powdered titania, *Langmuir* 4 (1988) 1156–1159.
- [27] H. Yoneyama, S. Haga, S. Yamanaka, Photocatalytic activities of microcrystalline titania incorporated in sheet silicates of clay, *J. Phys. Chem.* 93 (1989) 4833–4837.
- [28] Y.I. Kim, S.W. Keller, J.S. Krueger, E.H. Yonemoto, G.B. Saupe, T.E. Mallouk, Photochemical charge transfer and hydrogen evolution mediated by oxide semiconductor particles in zeolite-based molecular assemblies, *J. Phys. Chem.* 101 (1997) 2491–2500.
- [29] R.J. Tayade, R.G. Kulkarni, R.V. Jasra, Transition metal ion impregnated mesoporous TiO₂ for photocatalytic degradation of organic contaminants in water, *Ind. Eng. Chem. Res.* 45 (2006) 5231–5238.
- [30] Y.M. Xu, P.E. Ménassa, C.H. Langford, Photodecomposition of several chloroaromatics using a commercial prototype reactor, *Chemosphere* 17 (1988) 1971–1976.
- [31] R.W. Matthews, Solar-electric water purification using photocatalytic oxidation with TiO₂ as a stationary phase, *Sol. Energy* 38 (1987) 405–413.
- [32] K. Vinodgopal, S. Hotchandani, P.V. Kamat, Electrochemically assisted photocatalysis: Titania particulate film electrodes for photocatalytic degradation of 4-chlorophenol, *J. Phys. Chem.* 97 (1993) 9040–9044.
- [33] P.K. Surolia, R.J. Tayade, R.V. Jasra, TiO₂-coated cenospheres as catalysts for photocatalytic degradation of methylene blue, p-nitroaniline, n-decane, and n-tridecane under solar irradiation, *Ind. Eng. Chem. Res.* 49 (2010) 8908–8919.
- [34] I. Tiscornia, S. Irusta, P. Pradanos, C. Tellez, J. Coronas, J. Santamaria, Preparation and characterization of titanosilicate Ag-ETS-10 for propylene and propane adsorption, *J. Phys. Chem. C* 111 (2007) 4702–4709.
- [35] S.M. Kuznicki, V.A. Bell, S. Nair, H.W. Hillhouse, R.M. Jacubinas, C.M. Braunbarth, B.H. Toby, M. Tsapatsis, A titanosilicate molecular sieve with adjustable pores for size-selective adsorption of molecules, *Nature* 412 (2001) 720–724.
- [36] C. Lamberti, Electron-hole reduced effective mass in monoatomic ...-O-Ti-O-Ti-O-... quantum wires embedded in the siliceous crystalline matrix of ETS-10, *Microporous Mesoporous Mater.* 30 (1999) 155–163.
- [37] S. Bordiga, G.T. Turnes Palomino, A. Zecchina, G. Ranghino, E. Giamello, C. Lamberti, Stoichiometric and sodium-doped titanium silicate molecular sieve containing atomically defined -OTiOTiO- chains: Quantum *ab initio* calculations, spectroscopic properties, and reactivity, *J. Chem. Phys.* 112 (2000) 3859–3867.
- [38] P.K. Surolia, R.J. Tayade, R.V. Jasra, Photocatalytic degradation of nitrobenzene in an aqueous system by transition-metal-exchanged ETS-10 Zeolites, *Ind. Eng. Chem. Res.* 49 (2010) 3961–3966.
- [39] G.Q. Guan, T. Kida, K. Kusakabe, K. Kimura, E. Abe, A. Yoshida, Photocatalytic reactivity of noble metal-loaded ETS-4 zeolites, *Inorg. Chem. Commun.* 7 (2004) 618–620.
- [40] S.M. Kuznicki, Large-pored crystalline titanium molecular sieve zeolites, US Patent 4853202 A, 1989.
- [41] S. Nair, M. Tsapatsis, B.H. Toby, S.M. Kuznicki, A Study of heat-treatment induced framework contraction in strontium-ETS-4 by powder neutron diffraction and vibrational spectroscopy, *J. Am. Chem. Soc.* 123 (2001) 12781–12790.
- [42] R.S. Pillai, S.A. Peter, R.V. Jasra, Adsorption of carbon dioxide, methane, nitrogen, oxygen and argon in NaETS-4, *Microporous Mesoporous Mater.* 113 (2008) 268–276.

- [43] R.P. Marathe, S. Farooq, M.P. Srinivasan, Modeling gas adsorption and transport in small-pore titanium silicates, *Langmuir* 21 (2005) 4532–4546.
- [44] M.C. Mitchell, M. Gallo, T.M. Nenoff, Computer simulations of adsorption and diffusion for binary mixtures of methane and hydrogen in titanosilicates, *J. Chem. Phys.* 121 (2004) 1910–1916.
- [45] H. Yamashita, M. Matsuoka, M. Anpo, M. Che, XAFS studies on the metal ion (Cu, Ag) photocatalysts prepared within zeolite cavities using an ion-exchange method, *J. Phys. Chem. B* 7 (1997) 941–942.
- [46] S.M. Kanan, M.A. Omary, H.H. Patterson, M. Matsuoka, M. Anpo, Characterization of the excited states responsible for the action of silver(I)-doped ZSM-5 zeolites as photocatalysts for nitric oxide decomposition, *J. Phys. Chem. B* 104 (2000) 3507–3517.
- [47] M. Anpo, S.G. Zhang, H. Mishima, M. Matsuoka, H. Yamashita, Design of photocatalysts encapsulated within the zeolite framework and cavities for the decomposition of NO into N₂ and O₂ at normal temperature, *Catal. Today* 39 (1997) 159–168.
- [48] U.G. Akpan, B.H. Hameed, Development and photocatalytic activities of TiO₂ doped with Ca–Ce–W in the degradation of acid red 1 under visible light irradiation, *Desalin. Water Treat.* 52 (2013) 5639–5651.
- [49] H.Y. Yang, F. Chen, Y.C. Jiao, J.L. Zhang, The role of interfacial lattice Ag⁺ on titania based photocatalysis, *Appl. Catal., B Environ.* 130–131 (2013) 218–223.
- [50] M. Ni, M.K.H. Leung, D.Y.C. Leung, K. Sumathy, A review and recent developments in photocatalytic water-splitting using TiO₂ for hydrogen production, *Renewable Sustainable Energy Rev.* 11 (2007) 401–425.
- [51] M. Khairy, W. Zakaria, Effect of metal-doping of TiO₂ nanoparticles on their photocatalytic activities toward removal of organic dyes, *Egypt. J. Pet.* 23 (2014) 419–426.
- [52] K.P. Prasanth, H.C. Bajaj, H.D. Chung, K.Y. Choo, T.H. Kim, R.V. Jasra, Hydrogen sorption in transition metal modified NaETS-4, *J. Alloys Compd.* 480 (2009) 580–586.
- [53] R.J. Tayade, R.G. Kulkarni, R.V. Jasra, Photocatalytic degradation of aqueous nitrobenzene by nanocrystalline TiO₂, *Ind. Eng. Chem. Res.* 45 (2006) 922–927.
- [54] L. Rizzo, S. Meric, D. Kassinos, M. Guida, F. Russo, V. Belgiorno, Degradation of diclofenac by TiO₂ photocatalysis: UV absorbance kinetics and process evaluation through a set of toxicity bioassays, *Water Res.* 43 (2009) 979–988.
- [55] M.C. Hasegawa, J.F.d.S. Daniel, K. Takashima, G.A. Batista, S.M.C.P. da Silva, COD removal and toxicity decrease from tannery wastewater by zinc oxide-assisted photocatalysis: A case study, *Environ. Technol.* 35 (2014) 1589–1595.
- [56] S.S. Shinde, C.H. Bhosale, K.Y. Rajpure, Kinetic analysis of heterogeneous photocatalysis: Role of hydroxyl radicals, *Catal. Rev.* 55 (2013) 79–133.
- [57] M. Naderi, M.W. Anderson, Phase transformation of microporous titanosilicate ETS-4 into narsarsukite, *Zeolites* 17 (1996) 437–443.
- [58] B. Mihailova, V. Valtchev, S. Mintova, L. Konstantinov, Vibrational spectra of ETS-4 and ETS-10, *Zeolites* 16 (1996) 22–24.
- [59] N.V. Zubkova, D.Y. Pushcharovsky, G. Giester, I.V. Pekov, A.G. Turchkova, N.V. Chukanov, E. Tillmanns, Crystal structures of K- and Cs-exchanged forms of zorite, *Crystallogr. Rep.* 50 (2005) 367–373.
- [60] R.P. Marathe, K. Mantri, M.P. Srinivasan, S. Farooq, Effect of ion exchange and dehydration temperature on the adsorption and diffusion of gases in ETS-4, *Ind. Eng. Chem. Res.* 43 (2004) 5281–5290.
- [61] G.Q. Guan, T. Kida, K. Kusakabe, K. Kimura, X.M. Fang, T.L. Ma, E. Abe, A. Yoshida, Photocatalytic H₂ evolution under visible light irradiation on CdS/ETS-4 composite, *Chem. Phys. Lett.* 385 (2004) 319–322.
- [62] D.G. Gong, W.C.J. Ho, Y.X. Tang, Q. Tay, Y.K. Lai, J.G. Highfield, Z. Chen, Silver decorated titanate/titania nanostructures for efficient solar driven photocatalysis, *J. Solid State Chem.* 189 (2012) 117–122.
- [63] X.Y. Li, P.L. Yue, C. Kotal, Synthesis and photocatalytic oxidation properties of iron doped titanium dioxide nanosemiconductor particles, *New J. Chem.* 27 (2003) 1264–1269.
- [64] J.F. Zhu, W. Zheng, B. He, J.L. Zhang, M. Anpo, Characterization of Fe-TiO₂ photocatalysts synthesized by hydrothermal method and their photocatalytic reactivity for photodegradation of XRG dye diluted in water, *J. Mol. Catal. A: Chem.* 216 (2004) 35–43.
- [65] P.K. Surolia, R.J. Tayade, R.V. Jasra, Effect of anions on the photocatalytic activity of Fe(III) salts impregnated TiO₂, *Ind. Eng. Chem. Res.* 46 (2007) 6196–6203.
- [66] W.J. Kim, M.C. Lee, J.C. Yoo, D.T. Hayhurst, Study on the rapid crystallization of ETS-4 and ETS-10, *Microporous Mesoporous Mater.* 41 (2000) 79–88.
- [67] H.-I. Lee, J.-H. Kim, H.-S. Lee, W.-D. Lee, Purification of toxic compounds in water and treatment of polymeric materials, in: M. Anpo, P.V. Kamat (Eds.), *Environmentally Benign Photocatalysts*, Springer, New York, 2010, pp. 345–402.
- [68] S. Usseglio, P. Calza, A. Damin, C. Minero, S. Bordiga, C. Lamberti, E. Pelizzetti, A. Zecchina, Tailoring the selectivity of Ti-based photocatalysts (TiO₂ and microporous ETS-10 and ETS-4) by playing with surface morphology and electronic structure, *Chem. Mater.* 18 (2006) 3412–3424.
- [69] A. Kitiyanan, S. Yoshikawa, The use of ZrO₂ mixed TiO₂ nanostructures as efficient dye-sensitized solar cells' electrodes, *Mater. Lett.* 59 (2005) 4038–4040.
- [70] D. Vione, S. Khanra, S.C. Man, P.R. Maddigapu, R. Das, C. Arsene, R.I. Olariu, V. Maurino, C. Minero, Inhibition vs. enhancement of the nitrate-induced phototransformation of organic substrates by the ·OH scavengers bicarbonate and carbonate, *Water Res.* 43 (2009) 4718–4728.
- [71] J. Zhang, Y. Nosaka, Quantitative detection of OH radicals for investigating the reaction mechanism of various visible-light TiO₂ photocatalysts in aqueous suspension, *J. Phys. Chem. C* 117 (2013) 1383–1391.
- [72] Y. Nosaka, S. Komori, K. Yawata, T. Hirakawa, A.Y. Nosaka, Photocatalytic ·OH radical formation in TiO₂ aqueous suspension studied by several detection methods, *Phys. Chem. Chem. Phys.* 5 (2003) 4731–4735.
- [73] C.S. Turchi, D.F. Ollis, Photocatalytic degradation of organic water contaminants: Mechanisms involving hydroxyl radical attack, *J. Catal.* 122 (1990) 178–192.